

Decadal variability in twentieth-century ocean acidification in the California Current Ecosystem

Emily B. Osborne^{1,2*}, Robert C. Thunell^{3,6}, Nicolas Gruber⁴, Richard A. Feely⁵ and Claudia R. Benitez-Nelson³

Oceanic uptake of CO₂ can mitigate climate change, but also results in global ocean acidification. Ocean acidification-related changes to the marine carbonate system can disturb ecosystems and hinder calcification by some organisms. Here, we use the calcification response of planktonic foraminifera as a tool to reconstruct the progression of ocean acidification in the California Current Ecosystem through the twentieth century. Measurements of nearly 2,000 fossil foraminifera shell weights and areas preserved in a marine sediment core showed a 20% reduction in calcification by a surface-dwelling foraminifera species. Using modern calibrations, this response translates to an estimated 35% reduction in carbonate ion concentration, a biologically important chemical component of the carbonate system. Assuming other aspects of the carbonate system, this represents a 0.21 decline in pH, exceeding the estimated global average decline by more than a factor of two. Our proxy record also shows considerable variability that is significantly correlated with Pacific Decadal Oscillation and decadal-scale changes in upwelling strength, a relationship that until now has been obscured by the relatively short observational record. This modulation suggests that climatic variations will play an important role in amplifying or alleviating the anthropogenic signal and progression of ocean acidification in this region.

Since the beginning the industrial era, atmospheric CO₂ levels have risen from 280 ppm to more than 400 ppm; an unprecedented concentration over the past 800,000 years¹. The oceans have absorbed approximately 27% of this anthropogenic CO₂, which has caused an estimated 0.1 reduction in global mean surface ocean pH: the phenomenon known as ocean acidification^{2–6}. Field studies of some of the ocean's major calcium carbonate producing organisms often indicate a negative calcification response, declining [CO₃²⁻] (for example, refs. 7–15), although in some instances calcification remains unaffected or is even enhanced (for example, see refs. 14,15).

Research suggests that ocean acidification is becoming particularly acute in coastal upwelling regions, such as the California Current Ecosystem (CCE), due to their low buffering capacity and the natural upwelling processes that bring CO₂-rich intermediate waters to the ocean surface (for example, ref. 3,16–21). Models indicate a considerable decline in [CO₃²⁻] in the CCE and a shoaling of the saturation horizons for each of the CaCO₃ mineral polymorphs (calcite Ω_{cal} and aragonite Ω_{arg}) since the onset of the industrial period, reducing the volume of the surface ocean favourable for calcification^{20–22}. Modern sampling has identified malformed and dissolved aragonite-secreting pteropods during periods of strong upwelling, when the saturation horizon comes very close to (or even intersects with) the sea surface^{7,16,23}.

Initial surveys of the global ocean marine carbonate system only began in the late 1970s, well after anthropogenic carbon began altering the marine carbonate system²⁴. Within the CCE specifically, consistent in situ observations of carbonate system variables are limited to the last decade (from the California Cooperative Oceanic Fisheries Investigations (CalCOFI), 2009 to present). While these

observational records are critically important to our understanding of ocean chemistry, they do not provide a sufficiently long historical record of this phenomenon. The lack of long-term ocean acidification records limits our ability to place recent observations into the context of past change, and hinders an assessment of the impacts of natural decadal climate oscillations on the marine carbonate system. Model simulations can close the knowledge gap, but without constraints from in situ and/or proxy measurements, their validity remains unknown—especially with regard to their skill in capturing variability. Here, we provide a century-long, nearly annually resolved ocean acidification proxy record for the central region of the CCE and investigate the twentieth-century trends and decadal-scale processes at play.

Carbonate chemistry and calcification

A number of studies have demonstrated that the carbonate chemistry of seawater strongly influences the calcification of planktonic foraminifera, leaving a distinct imprint on the thickness of their shells. This has permitted researchers to use shell weight as a proxy for past surface ocean [CO₃²⁻]. However, shell weight also inherently reflects shell size, which is chiefly controlled by the ambient temperature, and perhaps other variables^{25–27} see Methods for extended discussion). Here, we use a relatively new shell weight technique²⁸ that effectively size-normalizes individual shell weights (Methods), called area normalized shell weight (ANSW), which can be used to quantitatively assess shell thickness and, by extension, [CO₃²⁻]. We apply this technique to the ubiquitously occurring surface-mixed-layer species *Globigerina bulloides* to reconstruct ambient-[CO₃²⁻] over the past 100 years, building on a proof of concept for this species and method by Osborne et al.²⁹ (Methods). Previous research

¹Ocean Acidification Program, National Oceanic and Atmospheric Administration, Silver Spring, MD, USA. ²Cooperative Program for the Advancement of Earth System Science, University Corporation for Atmospheric Research, Boulder, CO, USA. ³School of the Earth, Ocean and Environment, University of South Carolina, Columbia, SC, USA. ⁴Environmental Physics, Institute of Biogeochemistry and Pollutant Dynamics, ETH Zürich, Zurich, Switzerland.

⁵Pacific Marine Environmental Laboratory, National Oceanic and Atmospheric Administration, Seattle, WA, USA. ⁶Deceased: Robert C. Thunell.

*e-mail: emily.osborne@noaa.gov

on *G. bulloides* has suggested that the calcification and growth of this species might also be influenced by ambient temperature, nutrient concentration or 'optimal growth conditions'^{30–32}. The study by Osborne et al.²⁹ examined sediment trap collections and a sediment core record of *G. bulloides* shell weight, area and diameter data to closely evaluate these relationships and provided robust evidence that ANSW is directly controlled by ambient $[\text{CO}_3^{2-}]$, rather than by temperature or nutrient concentration ($R^2=0.80$ (where R is the coefficient of multiple correlation), standard error of the estimate = $\pm 16 \mu\text{mol kg}^{-1}$) (see Methods for discussion and Extended Data Fig. 1).

Here, the ANSW of nearly 2,000 individual *G. bulloides* shells were measured using 58 sediment samples from a 0.48-m-long box core collected in an anoxic region of the Santa Barbara Basin (SBB; $34^\circ 14' \text{N}$, $120^\circ 02' \text{W}$; 580 m water depth; Extended Data Fig. 2). A radioisotope-based age model was developed for this 100-year laminated and unbioturbated sediment core (1898–2006 ± 6 yr) (see Methods and ref.²⁹). Downcore ANSW and shell diameter measurements indicate that, on average, *G. bulloides* produced 20% thinner and 7% larger shells, respectively, by the close of the twentieth century relative to those from 1900 (Extended Data Figs. 3 and 4). To assess whether *G. bulloides* shell thickness (and by extension $[\text{CO}_3^{2-}]$) has declined significantly over the core record, we examine decadal population averages of ANSW (Fig. 1). These averages indicate that shell thicknesses from the 1990–2000 populations are significantly thinner than the 1900–1910 populations (95% confidence). The decline in ANSW is further apparent in scanning electron micrographs of the shell wall thicknesses from the top and bottom of the sediment core (Fig. 1). There is an apparent increase in the rate of change that occurs roughly between the first half and the second half of the core. This change in slope seems to be associated with a greater frequency of low $[\text{CO}_3^{2-}]$ events occurring in the more recent portion of the record, thereby reducing the overall average $[\text{CO}_3^{2-}]$ during the later interval. Several notable $[\text{CO}_3^{2-}]$ events recorded in our proxy record coincide with low $[\text{CO}_3^{2-}]$ outputs in SBB model simulations²⁹ and occur in association with the timing of several strong El Niño events (1982–1983, 1987–1988, 1997–1998).

By applying the ANSW– $[\text{CO}_3^{2-}]$ relationship presented by Osborne et al.²⁹ to our downcore ANSW measurements, we estimate that surface ocean $[\text{CO}_3^{2-}]$ in the SBB decreased by 35%, representing a net change of approximately $98 \pm 16 \mu\text{mol kg}^{-1}$ in $[\text{CO}_3^{2-}]$ over the twentieth century (from $271 \pm 16 \mu\text{mol kg}^{-1}$ in 1895 to $173 \pm 16 \mu\text{mol kg}^{-1}$ in 2000; Fig. 2). Recent in situ surface ocean $[\text{CO}_3^{2-}]$ measurements from the SBB in the NOAA's WCOA data (2011–2013) and taken by CalCOFI (2009–2015) are in excellent agreement with the forward-projected trend of our estimated $[\text{CO}_3^{2-}]$ values, even though these datasets do not temporally overlap. The time-series slopes, used to determine a decadal rate of change, recorded by our proxy reconstruction ($-9.992 \mu\text{mol kg}^{-1} \text{dec}^{-1}$) and the integrated CalCOFI and WCOA data ($-10.716 \mu\text{mol kg}^{-1} \text{dec}^{-1}$) are within error of one another. An additional comparison to the HOT dataset from the North Pacific³³ also shows a similar long-term decline ($-6.616 \mu\text{mol kg}^{-1} \text{dec}^{-1}$), albeit with significantly higher $[\text{CO}_3^{2-}]$ values and a lower rate of decline, illustrating the inherently low $[\text{CO}_3^{2-}]$ conditions in the CCE. Hindcast model simulations for the CCE indicate a long-term trend (-5.431 , -5.397 and $-4.949 \mu\text{mol kg}^{-1} \text{dec}^{-1}$ at 0, 30 and 50 m depth, respectively) that is also in agreement with our proxy record; however, simulations indicate overall lower rate of change and $[\text{CO}_3^{2-}]$ values relative to our ANSW-based estimates, which is probably a result of negative biases that exist in the model configuration employed (refs.^{20,22}, see Methods).

As the relative concentrations of the dissolved inorganic carbon (DIC) species in seawater (CO_2 , HCO_3^- , CO_3^{2-}) covary in a predictable way, so do the variables of the marine carbonate system (DIC, total alkalinity (TA), pH and the partial pressure of CO_2). We use an

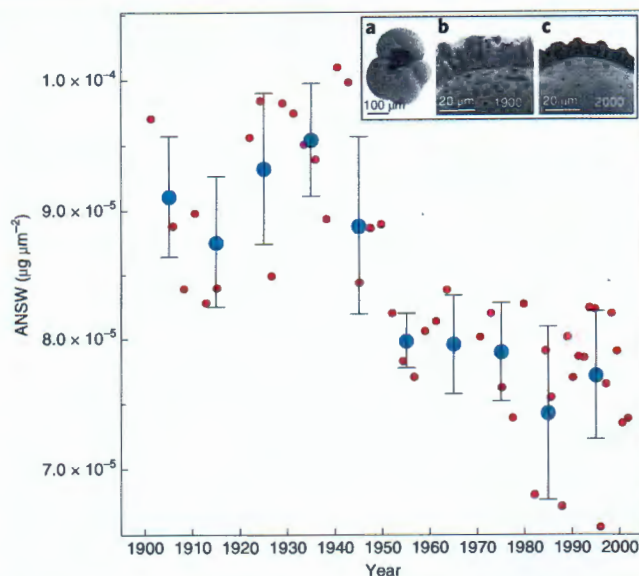


Fig. 1 | Decadal population mean ANSW. Red circles show the sample averages for the 58 sediment slices examined in this study. Decadal mean time-slice populations (blue circles) of *G. bulloides* ANSW show a significant offset in the shell thicknesses measured in 1900–1910 and 1990–2000. Error bars show the 95% confidence intervals. **a–c**, SEM images show a typical *G. bulloides* specimen from the SBB (**a**) and shell wall cross-sections of similarly sized shells from the upper- (**b**) and lower-most (**c**) samples of the box core, clearly illustrating the difference in shell wall thickness over the past century.

empirical salinity–TA relationship derived for the coastal zone of the CCE and sea surface salinity measurements from the Scripps Pier (1916–present) time series to estimate TA for our record³⁴. No salinity observations exist for the period 1895–1915; a best-fit linear regression is therefore used to estimate salinity values for those years. As this approach incorporates a great deal of uncertainty, particularly when applied to the palaeo record, we use a combination of our downcore proxy- $[\text{CO}_3^{2-}]$ and a salinity–TA estimates to roughly characterize the full carbonate system to report how the most commonly used measure of OA, pH, has evolved over the last century, so it can be compared with other published results (see Methods). These estimates indicate that the $[\text{H}^+]$ of seawater has increased by 80%, translating into a 0.21 unit decline in pH that exceeds the global average of 0.1 units by more than a factor of two³⁵. We do not report the error for this estimate, as a number of assumptions were made for these calculations and a reported value would probably underestimate uncertainty. However, our calculated decadal rate of pH decline for this region over the past century (-0.021dec^{-1}) is consistent with the rate of pH decline modelled for the entire CCE (-0.020dec^{-1} ; 1979–2012²⁰) and larger-scale observations for the North Pacific (-0.017dec^{-1} from 1991–2006³⁶ and -0.019dec^{-1} from 1988–2014; refs.^{33,37}). Our results are also consistent with large declines in pH resulting from strong upwelling, as is depicted by regional model simulations for the central region of the CCE^{20,21}.

Disentangling drivers of ocean acidification

The surface ocean carbonate system in our study region is influenced by a combination of exposure to atmospheric CO_2 , the local introduction of waters with low $[\text{CO}_3^{2-}]$ via shifts in upwelling and surface circulation, and local changes in productivity. To evaluate the dominating mechanism(s) driving the twentieth-century changes in the upper water column carbonate system, we use the

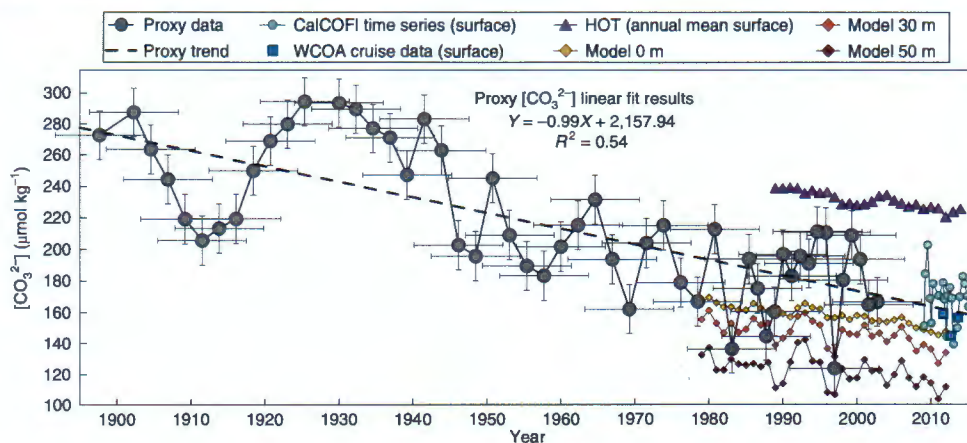


Fig. 2 | Twentieth-century proxy $[CO_3^{2-}]$ record based on *G. bulloides* NSW for the period 1895–2000. Horizontal error bars represent age uncertainty (± 6 yr) and vertical error bars ($\pm 15.63 \mu\text{mol kg}^{-1}$) represent the standard error of the estimate of $[CO_3^{2-}]$ associated with the calibration relationship²⁹. Proxy data are compared with model simulations (1979–2012 (ref. 20)), in situ measurements from the Santa Barbara Basin¹⁷ and HOT data from the North Pacific³³. The average modern $[CO_3^{2-}]$ is $164 \mu\text{mol kg}^{-1}$ and temperature is 15°C , based on 2010–2015 in situ data.

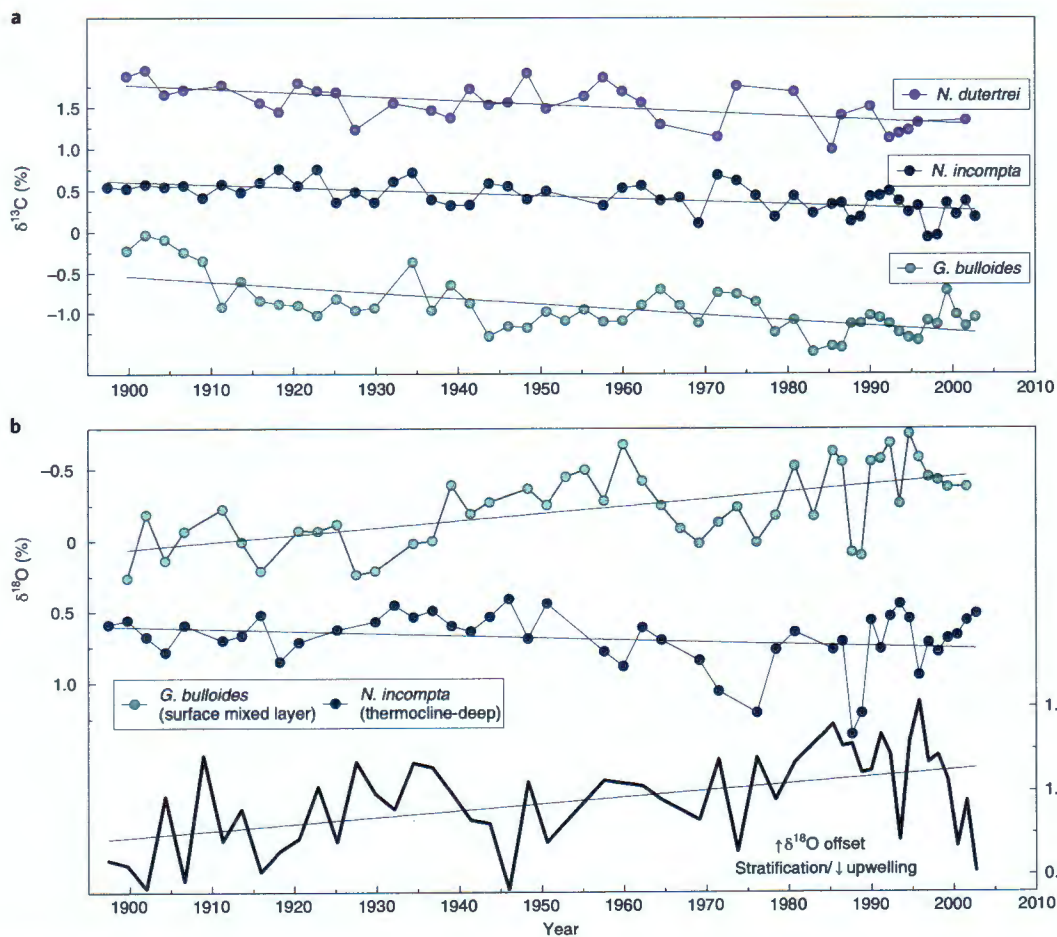


Fig. 3 | Stable isotope tracers of influential processes. **a**, The $\delta^{13}\text{C}$ records of three planktonic foraminifera species (*G. bulloides*, *N. incompta* and *N. dutertrei*; $R^2 = 0.46, 0.36$ and 0.34 , respectively, $P < 0.005$), showing a long-term decline consistent with an increasing anthropogenic CO_2 inventory in the surface ocean. **b**, The $\delta^{18}\text{O}$ records of *G. bulloides* (surface-mixed-layer-dwelling species) and *N. incompta* (thermocline-deep-dwelling species) (top), and the difference between the two records ($\Delta\delta^{18}\text{O}$) (bottom), which are used to trace the relative depth habitats and as a proxy for changes in the depth of the thermocline and the related thickness and stability of the mixed layer⁴⁵. $\delta^{18}\text{O}$ values are relative to the Vienna Pee Dee Belemnite.

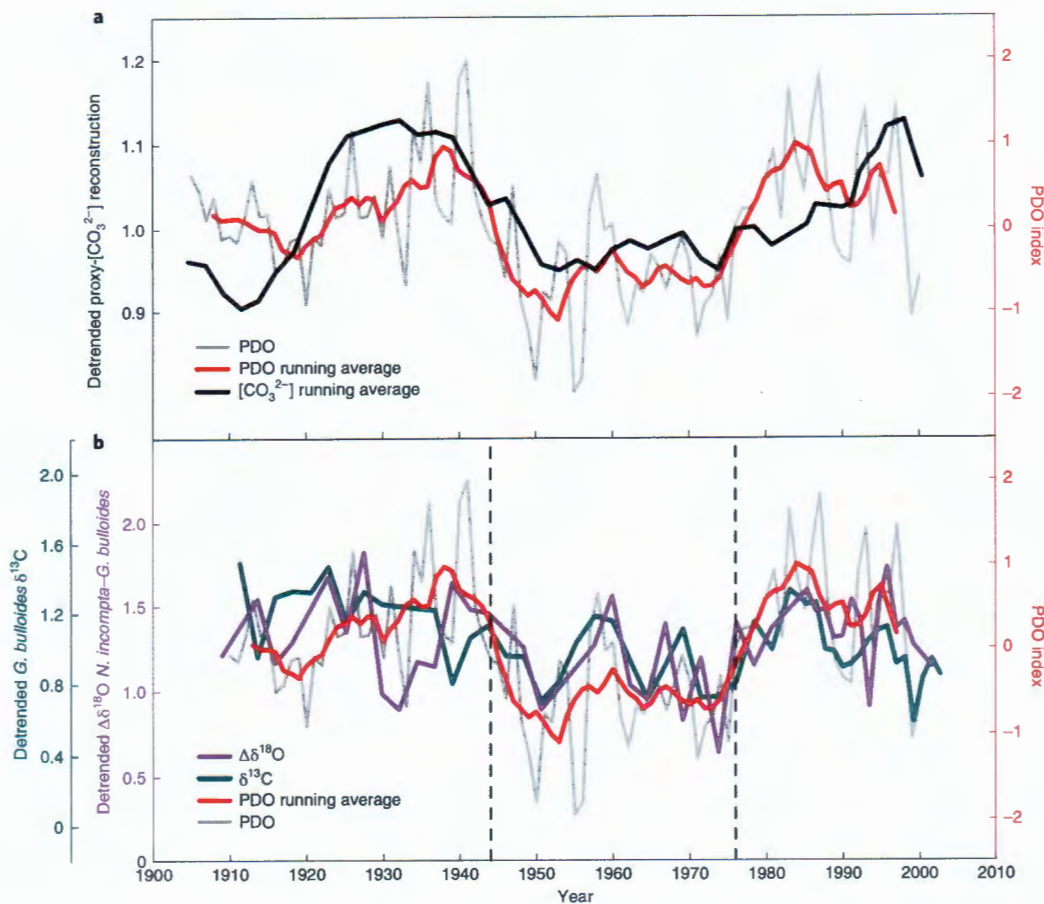


Fig. 4 | Linking upwelling strength, the PDO and carbonate system state. **a**, The $[CO_3^{2-}]$ record is shown, with the long-term, anthropogenically driven decline removed (detrended) plotted with the PDO index⁴⁸. An apparent correlation between high/low $[CO_3^{2-}]$ and positive/negative PDO phases is evident. Both datasets are shown as 5 yr running means. **b**, The detrended $\Delta\delta^{18}O$ (*N. incompta*–*G. bulloides*) and *G. bulloides* $\delta^{13}C$ are shown to highlight the natural variability not associated with anthropogenic ocean acidification, plotted again with the PDO index, indicating a relationship between weakened/strengthened upwelling and positive/negative PDO phases.

downcore foraminiferal stable isotopic records as tools to track carbon source and water column structure.

The $\delta^{13}C$ record of *G. bulloides* and two other foraminifera species (*Neogloboquadrina incompta* and *Neogloboquadrina dutertrei*) sampled from the core show significant ($R^2=0.46$, 0.36 and 0.34, respectively $P<0.005$) long-term declines in $\delta^{13}C$ (Fig. 3). The observed increase in the surface ocean inventory of anthropogenic carbon sourced from ^{12}C -enriched fossil fuels causes an overall decline in the $\delta^{13}C$ of seawater: a globally observed phenomenon termed the the Suess Effect^{38,39}. Variability in local productivity and upwelling of DIC- and ^{12}C -rich intermediate- and deep-water (from respiration and remineralization) could also influence the surface ocean, and (by extension) foraminiferal $\delta^{13}C$. The observed long-term decline in $\delta^{13}C$ is consistent with an increase in ^{13}C -depleted anthropogenic CO_2 , stemming primarily from uptake from the atmosphere, strengthened upwelling, a decline in productivity or a combination of these processes.

A $[CO_3^{2-}]$ effect has been observed in the stable isotope signatures recorded by foraminifera, whereby elevated $[CO_3^{2-}]$ results in relatively lower $\delta^{13}C$ (ref.²⁷). Considering the $[CO_3^{2-}]$ effect on foraminiferal $\delta^{13}C$, we estimate, on the basis of the culture-derived relationship of Spero et al.²⁷ for 13-chambered *G. bulloides* and the change in $[CO_3^{2-}]$ estimated by our proxy record, that $\delta^{13}C$ would increase by 0.94‰ from the years 1895 to 2000, whereas the measured decrease is $-0.72‰$. This modelled change in the opposite

direction is consistent with other, similar studies, and suggests that the magnitude of foraminiferal $\delta^{13}C$ depletion may actually be much larger when the $[CO_3^{2-}]$ effect is removed⁴⁰.

Considering the influence of upwelling on our $\delta^{13}C$ record, a majority of model evidence for the CCE suggests that coastal upwelling will be enhanced in coastal eastern boundary upwelling systems (EBUS) due to the climate-induced strengthening of alongshore winds that drive Ekman upwelling (for example, see ref.⁴¹). However, historical observations from the CalCOFI time series (1950–present) in the SBB report stratifying conditions over the latter half of the twentieth century associated with warming sea surface temperatures, deepening of the thermocline depth and declining zooplankton biomass^{42–44}. Using the $\Delta\delta^{18}O$ –water column structure proxy, we compare $\delta^{18}O$ signatures recorded by the surface-mixed-layer species (*G. bulloides*) with the thermocline to deep-dwelling foraminifera species (*N. incompta*) to infer the depth of the thermocline and the stability of the mixed layer⁴⁵. The observed increase in $\Delta\delta^{18}O$ represents an increasing offset in depth habitat and therefore a decline in upwelling strength, providing further evidence of twentieth-century CCE stratification, which would hypothetically result in an increase in $\delta^{13}C$ over our record, rather than the observed decrease (Fig. 3).

Shifts in dinoflagellate cyst assemblages in the SBB also suggest a reduction in upwelling and shed light on an overall reduction in seasonal primary productivity throughout the twentieth century⁴⁶.

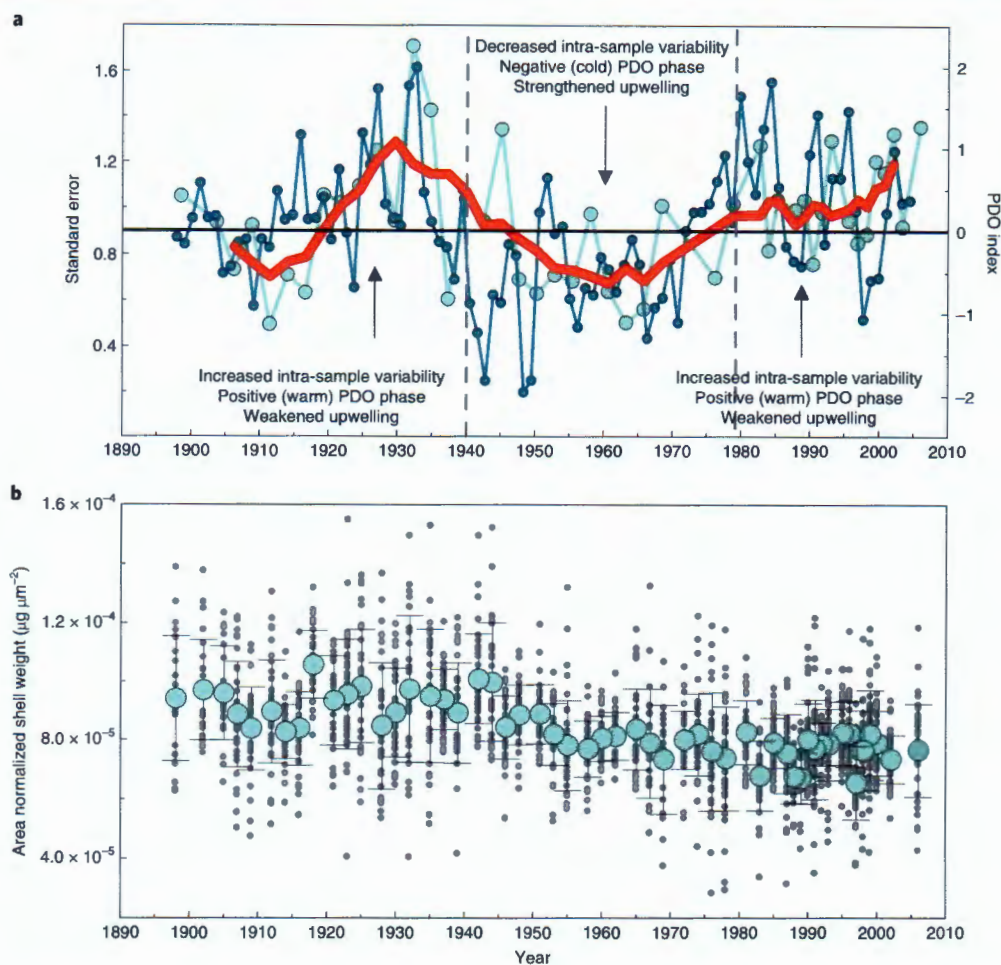


Fig. 5 | Using individuals to trace habitat depth and upwelling strength. a, Time series showing the sample ANSW standard error plotted (σ/\sqrt{n}) (n , sample size) with the PDO index. These time series show increased variability associated with positive PDO phases that are marked by weakened upwelling strength. The solid horizontal line correlates with the PDO index (right, y-axis) and delineates the threshold between positive and negative phases of PDO. Vertical dashed lines mark the temporal transitions between positive and negative phases of PDO based on the PDO index. **b**, Individual ANSW measurements (grey circles) plotted with sample average ANSW (blue circles) and associated sample standard error bars.

While this reduction in productivity is consistent with the sign of our $\delta^{13}\text{C}$ record, we argue that the magnitude of the productivity change is not great enough to persistently drive the observed $\delta^{13}\text{C}$ record. Productivity in the CCE and other EBUS may instead be a synergistic factor and important on shorter timescales.

Collectively, our records indicate that the increasing surface ocean inventory of anthropogenic CO_2 is the dominant long-term control on $\delta^{13}\text{C}$, and by extension $[\text{CO}_3^{2-}]$, recorded in our proxy record. This is supported by the fact that owing to a relatively robust scaling between the ^{13}C Suess effect and the increase in anthropogenic CO_2 of about -0.017 permil ($\mu\text{mol kg}^{-1}$)¹⁴⁷, the long-term decrease in $\delta^{13}\text{C}$ of about 0.72‰ over the 1895 to 2000 period implies an increase in anthropogenic CO_2 of about $42 \mu\text{mol kg}^{-1}$. This is slightly smaller than the expected increase of about $50 \mu\text{mol kg}^{-1}$ over this period, but supports our conclusion of a dominant contribution of the uptake of anthropogenic CO_2 to our reconstructed decrease in $[\text{CO}_3^{2-}]$.

Decadal-scale variability

While we attribute the long-term reduction in $[\text{CO}_3^{2-}]$ largely to air-sea exchange of anthropogenic CO_2 , considerable variability exists around the declining trend. To better visualize this variability, we detrended the $[\text{CO}_3^{2-}]$ record, revealing decadal-

subdecadal-scale oscillations that are significantly correlated with the Pacific Decadal Oscillation (PDO) index⁴⁸ ($R^2=0.53$, $P<0.005$; Extended Data Fig. 5) (Fig. 4). During positive (warm) phases of the PDO the carbonate system shifts to a higher $[\text{CO}_3^{2-}]$ state, whereas negative (cool) phases of the PDO coincide with overall lower $[\text{CO}_3^{2-}]$ values (Fig. 4a). PDO is associated with decadal-scale changes in the strength of the Aleutian Low, resulting in basin-wide temperature, pressure and wind stress anomalies in the Pacific Ocean⁴⁹. Within the CCE, the positive phase of the PDO coincides with weaker Aleutian Low winds, resulting in decreased coastal upwelling, warmer sea surface temperatures and reduced productivity. Conversely, the negative phase of the PDO produces the opposite set of conditions.

As coastal upwelling controls the amount of low-pH, CO_2 -rich water that reaches the surface, and PDO regulates the strength of upwelling, we hypothesize that this mechanism alters the surface carbonate system on decadal timescales. El Niño and La Niña events, typically lasting 6–18 months, produce similar anomalies and have already been observed in association with sustained changes in coastal upwelling and the acidity of surface waters off the continental shelf of California⁵⁰.

We use our detrended stable isotopic records ($\delta^{13}\text{C}$ and $\Delta\delta^{18}\text{O}$) to evaluate the variability occurring independently of the long-term

trend. We find that residual trends in $\delta^{13}\text{C}$ and $\Delta\delta^{18}\text{O}$ covary with the PDO: positive phases are marked by a higher $\Delta\delta^{18}\text{O}$ and $\delta^{13}\text{C}$ signatures, which represent decreased upwelling/increased stratification and warmer temperatures (Fig. 4). We also use the individual calcification response to assess upwelling variability on the basis of a similar foraminiferal depth habitat premise to the $\Delta\delta^{18}\text{O}$ proxy. During periods of strengthened upwelling, less intrasample variability is expected for a given *G. bulloides* population, since a shoaled thermocline would tighten the suitable habitable depth range for this species above the thermocline to the sea surface. The opposite would be true for stratified conditions. Using the sample population standard error as a measure of intrasample variability, a greater spread in individual ANSW is shown to be associated with intervals of positive PDO marked by weaker upwelling relative to negative PDO phases, when stronger upwelling occurs ($R^2=0.55$, $P<0.005$, Fig. 5 and Extended Data Fig. 5). Together, these proxy records corroborate that as upwelling weakens in the CCE during positive PDO phases, higher $[\text{CO}_3^{2-}]$ levels occur and during negative phases of the PDO, strengthened upwelling produces persistently lower $[\text{CO}_3^{2-}]$ conditions.

Implications for future ocean acidification

Our ocean acidification reconstruction indicates a significant long-term decline in $[\text{CO}_3^{2-}]$ of 35% recorded for the central CCE over the twentieth century as a result of increasing concentrations of anthropogenic CO_2 in seawater. Our ocean acidification record reveals considerable variability around this long-term trend, which we find to be significantly correlated with decadal-scale changes in upwelling strength associated with the PDO. This implies that over decadal timescales, the positive/negative phases of the PDO coincide with an overall elevated/reduced $[\text{CO}_3^{2-}]$ state as a result of shifts in upwelling strength. The relationship between the PDO and ocean acidification means that the anthropogenic acidification signal will be both amplified and alleviated in response to decadal shifts in the PDO phase, suggesting that that future progression of ocean acidification will be substantially modulated by large-scale climate modes. While projections of $[\text{CO}_3^{2-}]$ are important for understanding how the system may progress in the future, our past record indicates that $[\text{CO}_3^{2-}]$ will not decline linearly and that climatic forcing will be important in the coming century.

Online content

Any methods, additional references, Nature Research reporting summaries, source data, extended data, supplementary information, acknowledgements, peer review information; details of author contributions and competing interests; and statements of code and data availability are available at <https://doi.org/10.1038/s41561-019-0499-z>.

Received: 17 June 2019; Accepted: 6 November 2019;

Published online: 16 December 2019

References

- Lüthi, D. et al. High-resolution carbon dioxide concentration record 650,000–800,000 years before present. *Nature* **453**, 379–382 (2008).
- Feely, R. A. et al. Impact of anthropogenic CO_2 on the CaCO_3 system in the oceans. *Science* **305**, 362–366 (2004).
- Orr, J. C. et al. Anthropogenic ocean acidification over the twenty-first century and its impact on calcifying organisms. *Nature* **437**, 681–686 (2005).
- Gruber, N. et al. The ocean sink for anthropogenic CO_2 from 1994 to 2007. *Science* **363**, 1193–1199 (2019).
- Khatiwala, S. et al. Global ocean storage of anthropogenic carbon. *Biogeosciences* **10**, 2169–2191 (2013).
- Le Quéré, C. et al. Global carbon budget 2015. *Earth Syst. Sci. Data* **7**, 349–396 (2015).
- Bednaršek, N. et al. New ocean, new needs: application of pteropod shell dissolution as a biological indicator for marine resource management. *Ecol. Indic.* **76**, 240–244 (2017).
- de Moel, H. et al. Planktic foraminiferal shell thinning in the Arabian Sea due to anthropogenic ocean acidification? *Biogeosciences* **6**, 1917–1925 (2009).
- De'ath, G., Lough, J. M. & Fabricius, K. E. Declining coral calcification on the Great Barrier Reef. *Science* **342**, 116–119 (2009).
- Fabry, V. J., Seibel, B. A., Feely, R. A. & Orr, J. C. Impacts of ocean acidification on marine fauna and ecosystem processes. *ICES J. Mar. Sci.* **65**, 414–432 (2008).
- Meier, K. J. S., Beaufort, L., Heussner, S. & Ziveri, P. The role of ocean acidification in *Emiliana huxleyi* coccolith thinning in the Mediterranean Sea. *Biogeosciences* **11**, 2857–2869 (2014).
- Moy, A. D., Howard, W. R., Bray, S. G. & Trull, T. W. Reduced calcification in modern Southern Ocean planktonic foraminifera. *Nat. Geosci.* **2**, 276–280 (2009).
- Ries, J. B., Cohen, A. L. & McCorkle, D. C. Marine calcifiers exhibit mixed responses to CO_2 -induced ocean acidification. *Geology* **37**, 1131–1134 (2009).
- Rivero-Calle, S., Gnanadesikan, A., Del Castillo, C. E., Balch, W. M. & Guikema, S. D. Multidecadal increase in North Atlantic coccolithophores and the potential role of rising CO_2 . *Science* **350**, 1533–1537 (2015).
- Iglesias-Rodriguez, D. et al. Phytoplankton calcification in a high- CO_2 world. *Science* **320**, 336–340 (2008).
- Feely, R. A., Sabine, C. L., Hernandez-Ayon, J. M., Janson, D. & Hales, B. Evidence for upwelling of corrosive 'acidified' water onto the continental shelf. *Science* **320**, 1490–1492 (2008).
- Feely, R. A. et al. Chemical and biological impacts of ocean acidification along the west coast of North America. *Estuar. Coast. Shelf Sci.* **183**, 260–270 (2016).
- Feely, R. A. et al. The combined effects of acidification and hypoxia on pH and aragonite saturation in the coastal waters of the Californian Current Ecosystem and the northern Gulf of Mexico. *Cont. Shelf Res.* **152**, 50–60 (2018).
- Hauri, C. et al. Ocean acidification in the California Current System. *Oceanography* **22**, 60–71 (2009).
- Turi, G., Lachkar, Z., Gruber, N. & Munnich, M. Climatic modulation of recent trends in ocean acidification in the California Current System. *Environ. Res. Lett.* **11**, 014007 (2016).
- Gruber, N. et al. Rapid progression of ocean acidification in the California Current System. *Science* **337**, 220–223 (2012).
- Hauri, C., Gruber, N., McDonnell, A. M. P. & Vogt, M. The intensity duration and severity of low aragonite saturation state events on the California continental shelf. *Geophys. Res. Lett.* **40**, 3424–3429 (2013).
- Bednaršek, N. et al. *Limacina helicina* shell dissolution as an indicator of declining habitat suitability due to ocean acidification in the California Current Ecosystem. *Proc. R. Soc. Lond. B* **281**, 20140123 (2014).
- Takahashi, T., Williams, R. T. & Bos, D. L. in *GEOSECS Pacific Expedition Volume 3: Hydrographic Data 1973–1974* (eds Broecker, W. S. et al.) 77–83 (National Science Foundation, 1982).
- Barker, S. & Elderfield, H. Foraminiferal calcification response to glacial-interglacial changes in atmospheric CO_2 . *Science* **297**, 833–836 (2002).
- Bijma, J., Spero, H. J. & Lea, D. W. in *Use of Proxies in Paleoceanography: Examples from the South Atlantic* (eds Fisher, G. & Wefer, G.) 489–512 (Springer, 1999).
- Spero, H. J., Bijma, J., Lea, D. W. & Bemis, B. E. Effect of seawater carbonate concentration on foraminiferal carbon and oxygen isotopes. *Nature* **390**, 497–500 (1997).
- Marshall, B. J., Thunell, R., Hennehan, M., Astor, Y. & Wejnert, K. Planktonic foraminiferal area density as a proxy for carbonate ion concentration: a calibration study using the Cariaco Basin ocean time series. *Paleoceanography* **28**, 363–376 (2013).
- Osborne, E. B. et al. Calcification of the planktonic foraminifera *Globigerina bulloides* and carbonate ion concentration: results from the Santa Barbara Basin. *Paleoceanography* **31**, 1083–1102 (2016).
- Aldridge, D., Beer, C. J. & Purdie, D. A. Calcification in the planktonic foraminifera *Globigerina bulloides* linked to phosphate concentrations in surface waters of the North Atlantic Ocean. *Biogeosciences* **9**, 1725–1739 (2012).
- Beer, C. J., Schiebel, R. & Wilson, P. A. Testing planktic foraminiferal shell weight as a surface water $[\text{CO}_3^{2-}]$ proxy using plankton net samples. *Geology* **38**, 103–106 (2010).
- De Villiers, S. Optimum growth conditions as opposed to calcite saturation as a control on the calcification rate and shell-weight of marine foraminifera. *Mar. Biol.* **144**, 45–49 (2004).
- Dore, J. E., Lukas, R., Sadler, D. W., Church, M. J. & Karl, D. M. Physical and biogeochemical modulation of ocean acidification in the central North Pacific. *Proc. Natl Acad. Sci. USA* **106**, 12235–12240 (2009).
- Fassbender, A. J. et al. Estimating total alkalinity in the Washington State Coastal Zone: complexities and surprising utility for ocean acidification research. *Estuar. Coasts* **40**, 404–418 (2016).
- Caldeira, K. & Wickett, M. E. Anthropogenic carbon and ocean pH. *Nature* **425**, 365 (2003).

36. Byrne, R. H., Mecking, S., Feely, R. A. & Liu, X. Direct observations of basin-wide acidification of the North Pacific Ocean. *Geophys. Res. Lett.* **37**, L02601 (2010).
37. Bates, N. et al. A time-series view of changing ocean chemistry due to ocean uptake of anthropogenic CO₂ and ocean acidification. *Oceanography* **27**, 126–141 (2014).
38. Gruber, N. et al. Spatiotemporal patterns of carbon-13 in the global surface oceans and the oceanic Suess effect. *Glob. Biogeochem. Cycles* **13**, 307–335 (1999).
39. Keeling, C. D. The Suess effect: ¹³carbon-¹⁴carbon interrelations. *Environ. Int.* **2**, 229–300 (1979).
40. Black, D., Thunell, R. C., Wejnert, K. & Astor, Y. Carbon isotope composition of Caribbean sea surface waters: response to the uptake of anthropogenic CO₂. *Geophys. Res. Lett.* <https://doi.org/10.1029/2011GL048538> (2011).
41. Sydeeman, W. J. et al. Climate change and wind intensification in coastal upwelling ecosystems. *Science* **345**, 77–80 (2014).
42. Di Lorenzo, E., Miller, A. J. & SchneiderNand McWilliams, J. C. The warming of the California Current System: dynamics and ecosystem implications. *J. Phys. Oceanogr.* **35**, 336–362 (2005).
43. McGowan, J., Bograd, S., Lynn, R. J. & Miller, A. J. The biological response to the 1977 regime shift in the California Current. *Deep Sea Res. Pt II* **50**, 2567–2582 (2003).
44. Roemmich, D. & McGowan, J. Climatic warming and the decline of zooplankton in the California Current. *Science* **267**, 1324–1326 (1995).
45. Pak, D. K. & Kennett, J. P. A foraminiferal isotopic proxy for upper water mass stratification. *J. Foram. Res.* **32**, 319–327 (2002).
46. Bringue, M., Pospelova, V. & Field, D. B. High resolution sedimentary record of dinoflagellate cysts reflects decadal variability and 20th century warming in the Santa Barbara Basin. *Quat. Sci. Rev.* **105**, 86–101 (2014).
47. Sonnerup, R. E. & Quay, P. D. ¹³C constraints on ocean carbon cycle models. *Glob. Biogeochem. Cycles* **26**, GB2014 (2012).
48. Hare, S. R. *Low Frequency Climate Variability and Salmon Production*. PhD thesis, Univ. Washington (1996).
49. Mantua, N. J. & Hare, S. R. The Pacific Decadal Oscillation. *J. Oceanogr.* **58**, 35–44 (2002).
50. Nam, S., Kim, H.-J. & Send, U. Amplification of hypoxic and acidic events by La Niña conditions on the continental shelf off California. *Geophys. Res. Lett.* **120**, 5387–5399 (2015).

Publisher's note Springer Nature remains neutral with regard to jurisdictional claims in published maps and institutional affiliations.

This is a U.S. government work and not under copyright protection in the U.S.; foreign copyright protection may apply 2019

Methods

ANSW. While several shell weight size-normalization techniques used to estimate foraminiferal calcification and shell thickness exist, we chose to use ANSW, which uses individual (rather than bulk) population measurements²⁸. This method is currently the most effective size-normalization technique (compared with measure-based weights and sieve-based weights) that best constrains shell thickness^{28,29}. The inability to effectively size-normalize shell weight measurements results in datasets that are influenced not only by CO_3^{2-} but also by temperature, as temperature results in larger and heavier shells but has no effect on shell thickness. See Osborne et al.²⁹ for an in-depth discussion and review of previously published results for this species.

We aimed to pick 40 individual *G. bulloides* shells from the >150 μm size-fraction of each sediment sample for ANSW analyses. On average, 35 individuals are included in each ANSW data point (maximum 40 and minimum 17 individuals), representing a total of 1,870 analysed shells included in this dataset. Individual *G. bulloides* shells with abnormally formed shells or visible clay and/or organic material were excluded from our analyses, as these characteristics could affect weight and area measurements. The presence of an encrusted cryptic morphospecies of *G. bulloides* has been documented in the Santa Barbara Channel^{51–53}. Further investigation indicated that the less-abundant and cool-water-loving 'encrusted' morphospecies calcifies and fractionates stable carbon and oxygen isotopes differently to the more-abundant 'normal' morphospecies^{29,51}. Owing to the offset in ANSW and the intention to use these *G. bulloides* shells for later stable isotope analyses, morphometric measurements collected during ANSW processing are also used to identify and remove encrusted individuals from our sample populations (refs. 29,54). The species-specific ANSW response of the normal *G. bulloides* morphospecies to ambient $[\text{CO}_3^{2-}]$ has been constrained using individuals collected in the SBB by a sediment trap time series (equation (2)). Stable isotope results from this 3.5 yr sediment-trap analysis indicate that, on average, *G. bulloides* calcifies in the 40 m depth range, although seasonal variability in depth habit does occur in association with upwelling.

While there can still be a considerable amount of variability within a single sediment sample, statistical analyses by Osborne et al.²⁹ demonstrate the asymptotic nature of the per cent error as a function of the numbers of individuals used in an ANSW measurement. These results suggest that a pool of 30–40 individuals represents a high degree of confidence when using a mean area density value to represent the population mean. Each shell is individually weighed in a copper weigh boat using a high-precision microbalance (Mettler Toledo XP2U, $\pm 0.43 \mu\text{g}$) in an environmentally controlled weigh room. Next, each individual is photographed positioned umbilical side up using a binocular microscope (Zeiss Stemi 2000-C) fitted with a camera (Point Grey Research Flea3 1394b). A microscopic imaging program (Orbicle Macnification 2.0) was used to analyse shells photos for length (Feret diameter) and the two-dimensional surface area or silhouette. Macnification 2.0 program the RGB images to calculate a region of interest and generates an outline of the shell image, which is then used to estimate a pixel two-dimensional area. Pixel measurements are converted to lengths (μm) and areas (μm^2) by calibrating an image of a 1 mm microscale taken at the same magnification and working distance as the shell photos. Individual shell weights were then divided by their corresponding areas and a mean ANSW value was calculated for each sample population. These ANSW values were then applied to the calibration relation relationship (equation (1)) presented by Osborne et al.²⁹ to estimate $[\text{CO}_3^{2-}]$.

$$[\text{CO}_3^{2-}] = (\text{ANSW} - 4.19 \times 10^{-5}) / 1.92 \times 10^{-7} \quad (1)$$

Age model development. Approximately 2 g from each sample were freeze-dried and used for radioisotope measurements. Wet weights (recorded before freeze-drying) and dry weights were used to estimate the sample porosity and correct for compaction. Freeze-dried sediments were ground, loaded into counting vials and sealed with epoxy for 3 weeks before counting. Each sample was measured (3–5 days) for ^{210}Pb , ^{214}Pb and ^{137}Cs via gamma-decay counting using a high-purity germanium well detector⁵⁵.

The excess ^{210}Pb ($^{210}\text{Pb}_{\text{ex}}$), reflective of atmospheric deposition, rather than supported ^{210}Pb ($^{210}\text{Pb}_{\text{supp}}$) from the decay of ^{226}Ra , was determined by subtracting the activity of ^{214}Pb (assumed to be in secular equilibrium with $^{210}\text{Pb}_{\text{supp}}$; mean 3.7 dpm g^{-1}) from the activity of ^{210}Pb . The exponential decay of $^{210}\text{Pb}_{\text{ex}}$ observed in the core sediments (Fig. 3) was used to determine ages for the core using a combination of constant initial concentration (CIC) and constant rate of ^{210}Pb supply (CRS) models. An offset of approximately ± 1 yr was observed between models. Using these age constraints, an average sedimentation rate of 0.43 cm yr^{-1} , and an average mass accumulation rate of $5.84 \text{ g cm}^{-2} \text{ yr}^{-1}$, were determined for the core. The sedimentation rate determined from the $^{210}\text{Pb}_{\text{ex}}$ is relatively uniform over the entire 0.5 m core and is also in good agreement with previously determined radioisotope chronologies for the SBB^{56–58}. The increase in ^{137}Cs activity at 19 cm (Fig. 3) is used as an independent age marker horizon for the year 1964, and represents the peak in radioactive fallout from atmospheric nuclear bomb testing^{59,60}. The depth of the ^{137}Cs spike was shallower than expected using both the CRS and CIC models when assuming a 2012 collection year as the core-top age.

We therefore conclude that the upper several centimetres of sediments were not preserved when this box core was collected. As such, we applied a 6 yr age correction, which is also used as the age error estimate, and anchored the 19 cm ^{137}Cs spike to a depositional year of 1964. These age constraints indicate that the 0.5 m core extends back to ~1895 and that the uppermost sediments contained in the core represent the year ~2006.

CCE marine carbonate system model simulation. The model-based estimates of the progression of the $[\text{CO}_3^{2-}]$ in the SBB stem from the simulations described in detail by Turi et al.²⁰. Annual mean data were extracted from the model at the four nearest gridpoints to the location of the core from various depths (0 m, 30 m, and 50 m). The model is based on the UCLA-ETH version of the Regional Oceanic Modeling System⁶¹, and includes a nitrogen-based nutrient–phytoplankton zooplankton–detritus model⁶² that was extended with a carbon module^{63,64}. The CalCS model setup employed here has a horizontal resolution of 5 km and 34 levels in the vertical, spans the entire US coast from about 30°N to 50°N and extends more than 1,300 km into the Pacific. The hindcast simulation (1979–2012) was forced at the surface with fluxes of heat and freshwater from ECMWF's ERA-Interim reanalysis⁶⁵. The boundary conditions at the lateral boundaries of the model consisted of a combination of climatological fields based on observations and time-varying anomaly fields derived from a global hindcast simulation with the NCAR CCSM3 model⁶⁶. The evaluation of the model simulated pH and Ω_{arag} with observations revealed that the model is capturing the large-scale offshore and depth gradients very well, but that it has a slight positive bias in the nearshore regions north of Point Conception²². Owing to the lack of in situ measurements from the SBB, no assessment could be undertaken in this part of the CalCS, but the comparison with the time-series records from Santa Monica Bay⁶⁷ suggests a slight overestimation of the modelled pH and Ω_{arag} in the upper ocean.

Stable isotope measurements. At least 100 μg (30–40 individuals) of *G. bulloides* used for ANSW analyses were pooled to measure the stable $\delta^{18}\text{O}$ and $\delta^{13}\text{C}$ isotopic compositions. Foraminifera were cleaned for 30 min in 3% H_2O_2 followed by a brief sonication and acetone rinse before analysis. Stable isotope measurements were carried out on an Isoprime isotope ratio mass spectrometer equipped with a carbonate preparation system. The long-term standard reproducibility is 0.07‰ for $\delta^{18}\text{O}$ and 0.06‰ for $\delta^{13}\text{C}$. Results are reported relative to the Vienna Pee Dee Belemnite.

Marine carbonate system calculations. Carbonate system variables for the historic record were determined using the CO2Sys Program (version 2.1). TA and DIC were used as master input variables (equations (2) and (3)) and in situ measurements of sea surface temperature and salinity as input conditions when data are available (Shore Stations Program). Sea surface salinity measurements from the Scripps Pier (1916–present) located just south of our study region and sea surface temperature measurements from the SBB (1955–present) were used for our calculations. A comparison of more recent salinity measurements from the SBB and Scripps Pier indicate that salinity values in these two regions are comparable. For the period 1916–1954, when SST was not measured in the SBB but was measured at Scripps Pier, we use an average offset between the overlapping periods of these datasets (1955–1900) to extrapolate an SST for the SBB. For the period 1900–1916 when there is no hydrographic data available, we use the time-integrated relationship for temperature and salinity to estimate these parameters.

We solve for our input master variables (TA and DIC) by coupling proxy $[\text{CO}_3^{2-}]$ estimates and a salinity-based estimate of TA²⁴. Although this salinity–alkalinity relationship was derived using carbonate system measurements for the coastal Oregon CCE, a compilation of CalCOFI data from the SBB yields a relationship that is within error of the published Fassbender et al.¹⁴ dataset. We also incorporate total boron into our estimate of TA, which was determined using the R program seacarb (Total Boron Package⁶⁸). To estimate DIC, we sum the estimated $[\text{CO}_3^{2-}]$ with the derived $[\text{HCO}_3^-]$ and assume that any concentration of CO_2 is less than 1% of DIC (ref. 69; equation (3)).

$$\text{TA} = [\text{HCO}_3^-] + 2[\text{CO}_3^{2-}] + [\text{B}(\text{OH})_4^-] \quad (2)$$

$$\text{DIC} = [\text{HCO}_3^-] + [\text{CO}_3^{2-}] \quad (3)$$

Data availability

The authors declare that the data supporting the findings of this study are available within the article. New data generated as a part of this study have been made publicly available via PANGAEA (PDI-21505; <https://doi.pangaea.de/10.1594/PANGAEA.909101>). Additional data related to this study are available from the corresponding author on request. Publicly available data used in this study are described below. Carbonate chemistry measurements made within the SBB were collected seasonally by the California Cooperative Oceanic Fisheries Investigations time-series (CalCOFI; <http://calcofi.org/>) and during several NOAA West Coast Ocean Acidification Cruises (WCOA; <https://www.nodc.noaa.gov/ocads/oceans/Coastal/WCOA.html>). Observational data from the Hawaii Ocean Time-series

program (HOT; <http://hahana.soest.hawaii.edu/hot/>) were also used. Shore Station Data (salinity; <https://shorestations.ucsd.edu/shore-stations-data/>) were used for carbonate system calculations.

References

51. Bemis, B. E., Spero, H. J. & Thunell, R. C. Using species-specific paleotemperature equations with foraminifera: a case study in the Southern California Bight. *Mar. Micropaleo.* **46**, 405–430 (2002).
52. Darling, K. F. et al. Molecular evidence for genetic mixing of Arctic and Antarctic subpolar populations of planktonic foraminifers. *Nature* **405**, 43–47 (2000).
53. Sautter, L. R. & Thunell, R. C. Seasonal variability in the $\delta^{18}\text{O}$ and $\delta^{13}\text{C}$ of planktonic foraminifera from an upwelling environment: sediment trap results from the San Pedro Basin, Southern California Bight. *Paleoceanography* **6**, 307–334 (1991).
54. Marshall, B. J. et al. Morphometric and stable isotopic differentiation of *Orbulina universa* morphotypes from the Cariaco Basin, Venezuela. *Mar. Micropaleo.* **120**, 46–64 (2015).
55. Moore, W. S. Radium isotope measurements using germanium detectors. *Nucl. Instrum. Methods Phys. Res.* **223**, 407–411 (1984).
56. Bruland, K. W. *Pb-210 Geochronology in the Coastal Marine Environment*. PhD thesis, Univ. California (1974).
57. Koide, M., Soutar, A. & Goldberg, E. D. Marine geochronology with ^{210}Pb . *Earth Planet. Sci. Lett.* **14**, 422–446 (1972).
58. Krishnaswami, S., Lai, D., Amin, S. & Soutar, A. Geochronological studies in Santa Barbara Basin: ^{55}Fe as a unique tracer for particulate settling. *Limnol. Oceanogr.* **18**, 763–770 (1973).
59. Carter, M. W. & Moghissi, A. A. Three decades of nuclear testing. *Health Phys.* **33**, 55–71 (1977).
60. Ritchie, J. C. & McHenry, J. R. Application of radioactive fallout Cesium-137 for measuring soil erosion and sediment accumulations rates and patterns: a review. *J. Environ. Qual.* **19**, 215–233 (1989).
61. Shchepetkin, A. F. & McWilliams, J. C. The regional oceanic modeling system (ROMS): a split-explicit, free-surface, topography-following-coordinate oceanic model. *Ocean Model.* **9**, 347–404 (2005).
62. Gruber, N. et al. Eddy-resolving simulation of plankton ecosystem dynamics in the California Current System. *Deep Sea Res. Pt I* **53**, 1483–1516 (2006).
63. Gruber, N. et al. Rapid progression of ocean acidification in the California Current System. *Science* **337**, 220–223 (2012).
64. Hauri, C. et al. Spatiotemporal variability and long-term trends of ocean acidification in the California Current System. *Biogeosciences* **10**, 193–216 (2013).
65. Dee, D. P. et al. The ERA-Interim reanalysis: configuration and performance of the data assimilation system. *Q. J. R. Meteorol. Soc.* **137**, 553–597 (2011).
66. Graven, H. D., Gruber, N., Key, R., Khatiwala, S. & Giraud, X. Changing controls on oceanic radiocarbon: new insights on shallow-to-deep ocean exchange and anthropogenic CO_2 uptake. *J. Geophys. Res.* <https://doi.org/10.1029/2012JC008074> (2012).
67. Leinweber, A. & Gruber, N. Variability and trends of ocean acidification in the Southern California current system: a timeseries from Santa Monica Bay. *J. Geophys. Res.* **118**, 3622–3633 (2013).
68. Lee, K., Kim, T.-W., Byrne, R. H. & Liu, Y.-M. The universal ratio of boron to chlorine for the North Pacific and North Atlantic Oceans. *Geochim. Cosmochim. Acta* **74**, 1801–1811 (2010).
69. Zeebe, R. E. & Wolf-Gladrow, D. A. (eds) in *CO_2 in Seawater: Equilibrium, Kinetics, Isotopes* Vol. 65, 346 (Elsevier, 2001).

Acknowledgements

We dedicate this manuscript to co-author Robert C. Thunell, a wonderful colleague, friend and mentor, who lost his battle to cancer on 30 July 2018. This research was supported in part by a National Science Foundation grant to R.C.T. (1631977) and the Johanna M. Resig Fellowship granted to E.B.O. by the Cushman Foundation. R.A.F. was supported by the NOAA Ocean Acidification Program (PMEL contribution number 4546). N.G. acknowledges the support of ETH Zürich and of the Swiss National Foundation through the XEBUS project. We thank D. Burdige from Old Dominion University for collecting the box core used in this study; E. Tappa for his assistance with IRMS analyses and sediment trap recovery and deployments in the SBB; and N. Umling, whose review and scientific discourse greatly improved this manuscript.

Author contributions

E.B.O. and R.C.T. conceived the study and wrote the initial draft of the paper. E.B.O. designed and performed the analyses and has led the revision of the paper. N.G. and R.A.F. provided model and in situ data and contributed substantially to the discussion and interpretation of the results and writing of the paper. C.R.B.-N. conducted radiochemistry analyses, produced an age model for the core and contributed to the interpretation and writing of the paper.

Competing interests

The authors declare no competing interests.

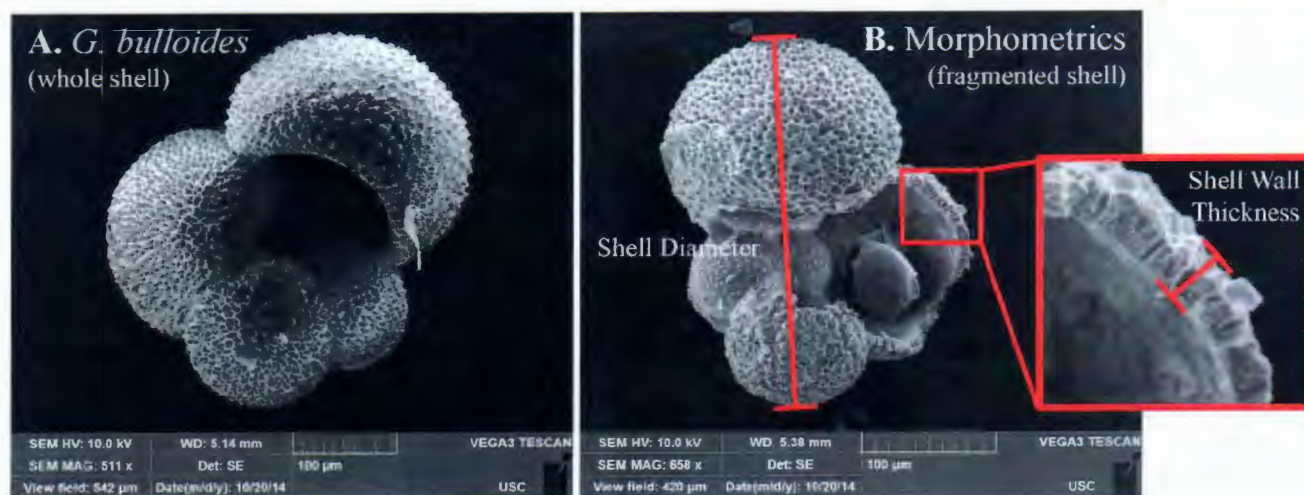
Additional information

Extended data is available for this paper at <https://doi.org/10.1038/s41561-019-0499-z>.

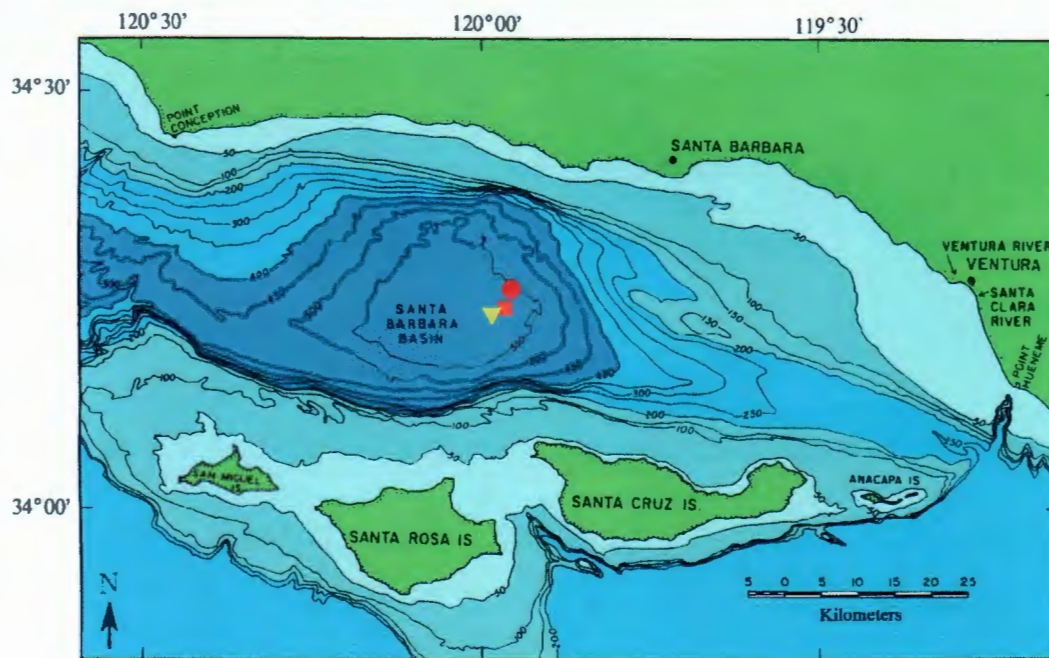
Correspondence and requests for materials should be addressed to E.B.O.

Peer review information Primary Handling Editor: James Super.

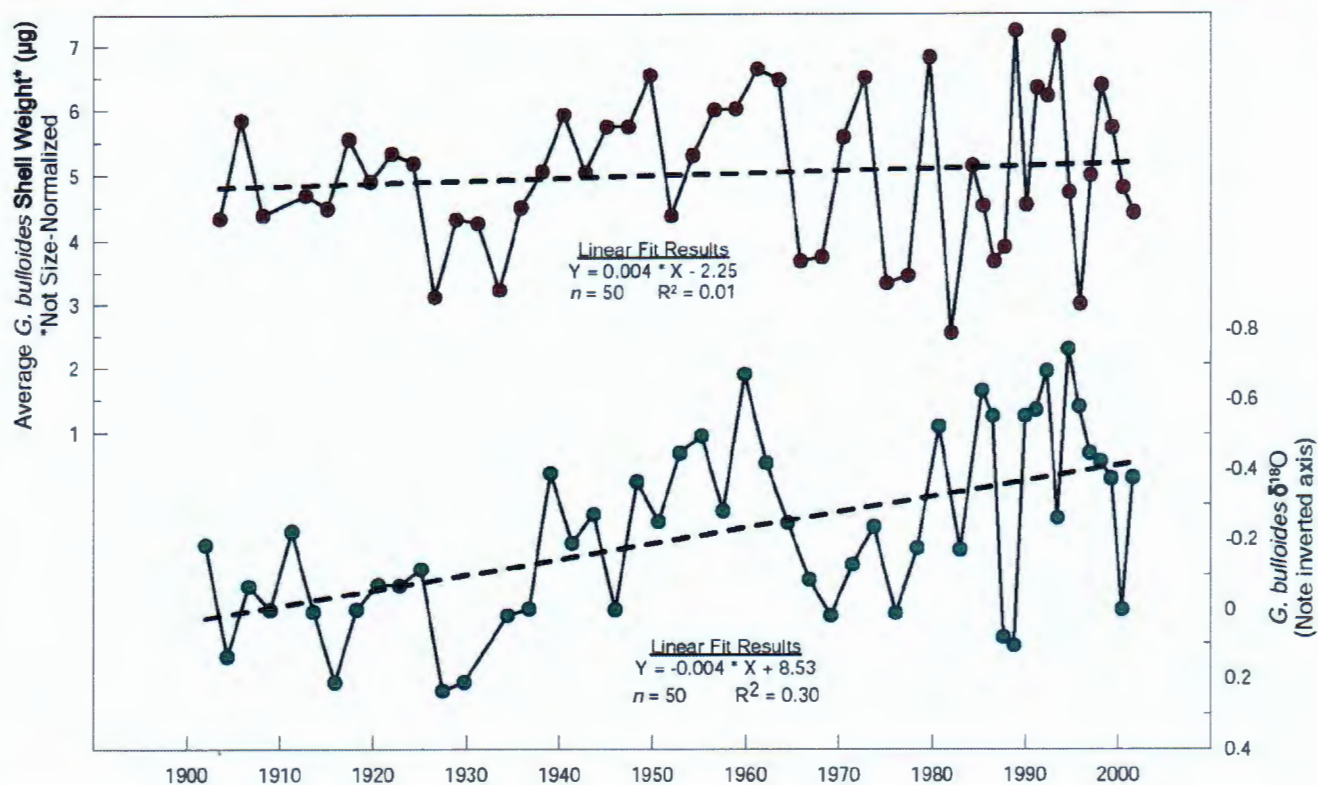
Reprints and permissions information is available at www.nature.com/reprints.



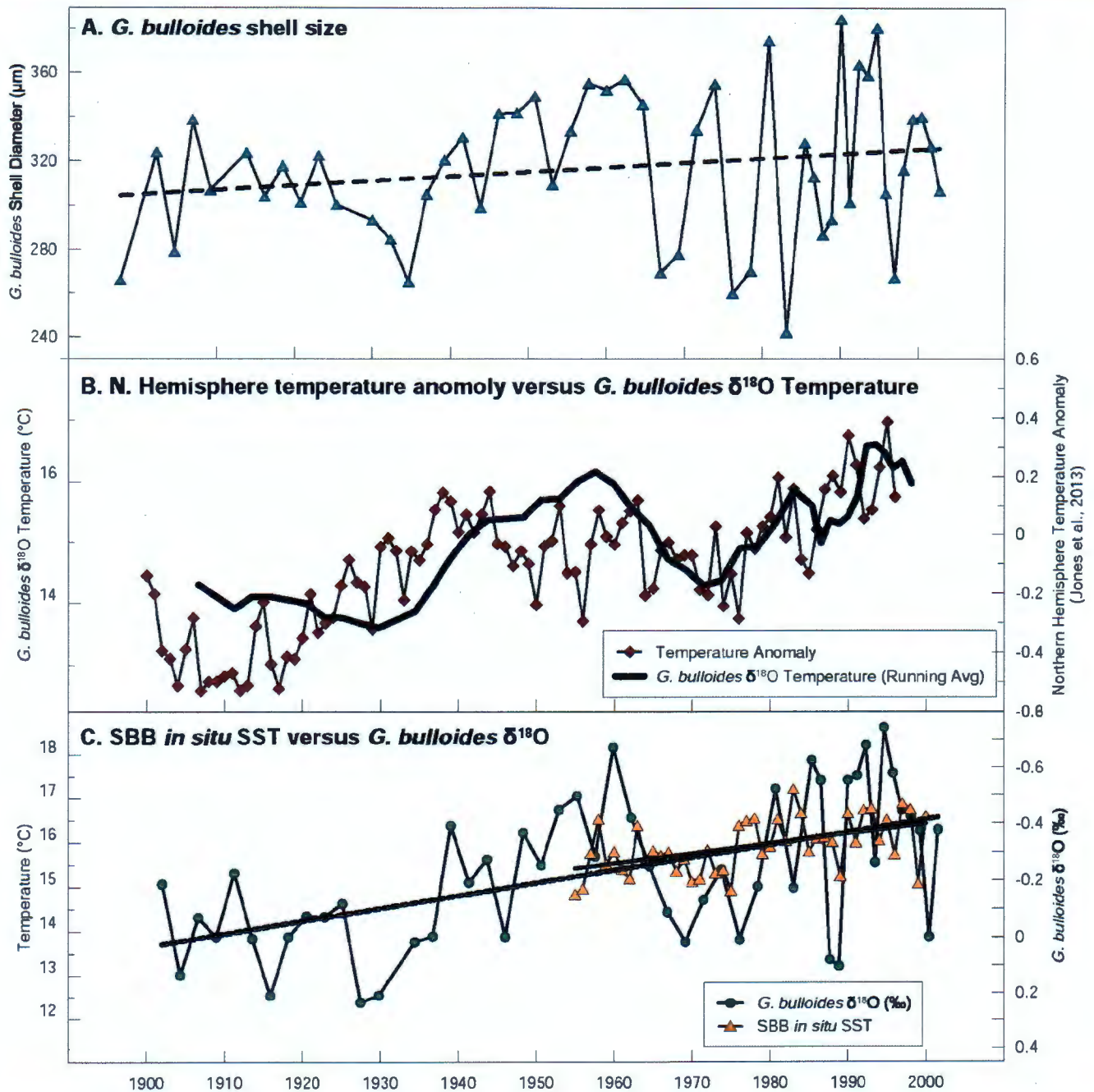
Extended Data Fig. 1 | Scanning Electron Microscope images of the study species, *G. bulloides*. B. *G. bulloides* shell with its final chamber broken showing a cross-sectional view of the shell wall, the key morphometric used in this study to estimate $[\text{CO}_3^{2-}]$. Shell wall thickness is indirectly estimated by measuring area normalized shell weight (ANSW: shell weight (μg) / 2-D surface area (μm^2)).



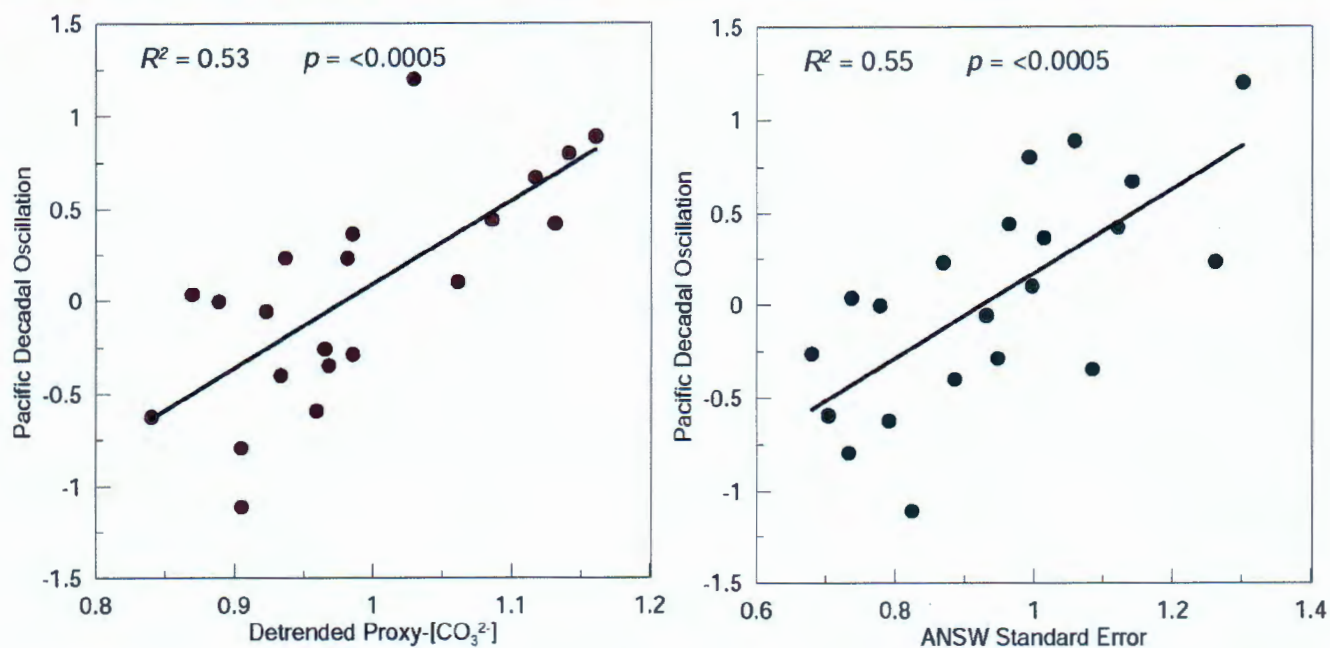
Extended Data Fig. 2 | Bathymetric map of the Santa Barbara Basin. The location of the box-core (red circle) used for the down-core reconstruction as well as the sediment trap (yellow triangle) and hydrographic sampling location (Plumes and Blooms Project Station 4; orange square) used in the calibration portion of the study²⁹.



Extended Data Fig. 3 | Down core trends in *G. bulloides* weight (not size-normalized) and $\delta^{18}O$. The increasing shell weight over the down core record coincides with a decline in $\delta^{18}O$ (note inverted axis), which represents an increase in temperature. This comparison provides a visualization of the importance of using size-normalized shell weights to estimate changes in calcification and shell thickness. Results from this study show that while overall shell weight and shell size are increasing as a result of warming temperatures, shell thickness is declining as a result of reduced [CO₃].



Extended Data Fig. 4 | The long-term shift in *G. bulloides* shell diameter increases in concert with warming sea surface temperatures. B. We compare the relative changes that are recorded *G. bulloides* $\delta^{18}\text{O}$ to a Northern Hemisphere Temperature anomaly for the 1900–2000 period and see a good agreement between temperature trends recorded in these records (Jones et al., 2013). **C.** We also compared *G. bulloides* $\delta^{18}\text{O}$ to in situ sea surface temperature (SST) measurements made in the Santa Barbara Basin (SBB; 1955–Present; Shore Stations Program) and see an excellent agreements between sea surface temperature and the $\delta^{18}\text{O}$ recorded in our *G. bulloides* shells.



Extended Data Fig. 5 | Time-series correlations between Pacific Decadal Oscillation Index and the detrended proxy-[CO₃²⁻] and ANSW sample standard error. Corresponding values were compared at 5-year time steps due to difference in time resolution across records. An independent t-test was conducted to compare both detrended proxy-[CO₃²⁻] and area-normalized shell weight standard area (a measure of sample variability) to the Pacific Decadal Oscillation Index. Highly significant correlation coefficients exist between PDO and the respective variables ($p < 0.005$) and the results of a paired t-tests for both records are highly significant ($p < 0.005$), further confirming significance of the relationships.